

**Recent Advances of Nonprecious and Bifunctional
Electrocatalysts for Overall Water Splitting**

Journal:	<i>Sustainable Energy & Fuels</i>
Manuscript ID	SE-REV-03-2020-000466.R1
Article Type:	Review Article
Date Submitted by the Author:	20-Apr-2020
Complete List of Authors:	Shang, Xiao; University of Cincinnati, Chemistry Tang, Jianhong; University of Cincinnati, Chemistry Dong, Bin; China University of Petroleum (East China) , State Key Laboratory; China University of Petroleum (East China) , College of Science Sun, Yujie; University of Cincinnati, Chemistry

Recent Advances of Nonprecious and Bifunctional Electrocatalysts for Overall Water Splitting

Xiao Shang,^a Jian-Hong Tang,^a Bin Dong,^{b,c*} Yujie Sun^{a*}

^aDepartment of Chemistry, University of Cincinnati, Cincinnati, OH 45221, USA

^bState Key Laboratory of Heavy Oil Processing, China University of Petroleum (East China), Qingdao 266580, PR China

^cCollege of Science, China University of Petroleum (East China), Qingdao 266580, PR China

Abstract

Electrocatalytic water splitting to produce clean hydrogen is a promising technique for renewable energy conversion and storage in the future energy portfolio. Aiming at industrial hydrogen production, cost-effective electrocatalysts are expected to be competent in both hydrogen evolution reaction (HER) and oxygen evolution reaction (OER) to accomplish the overall water splitting. Limited by the low tolerance and/or poor activity of most 1st-row transition metal-based electrocatalysts in strongly acidic media, the bifunctional electrocatalysts are currently advocated to work in high pH. Herein, this review summarizes recent progress of nonprecious bifunctional electrocatalysts for overall water splitting in alkaline media, including transition metal-based phosphides, chalcogenides, oxides, nitrides, carbides, borides, alloys, and metal-free materials. Besides, some prevalent modification strategies to optimize the activities of catalysts are briefly listed. Finally, the prospective on current challenges and future prospects for overall water splitting driven by advanced nonprecious electrocatalysts are briefly discussed.

Keywords: *nonprecious electrocatalysts; overall water splitting; transition metal; modification strategies*

1. Introduction

Electrocatalytic water splitting to produce clean hydrogen (H₂) has attracted intense interest during the last decade, in that H₂ is widely recognized as a green fuel, energy carrier, and plays an important role in the current chemical industry as well as future energy portfolio. The overall water splitting electrolysis can be divided into two half reactions, the cathodic hydrogen evolution reaction (HER) and the anodic oxygen evolution reaction (OER). Both half reactions involve multi electron transportation on intermediates, varied by the pH conditions as shown in Figure 1. The general mechanism of HER involves an electrochemical hydrogen adsorption step followed by an electrochemical desorption or recombination reaction.¹ In the case of OER, it involves the formation of adsorbed OH* on catalyst surface with subsequent transformation to OOH* and the eventual release of O₂.² The standard thermodynamic voltage to split water is 1.23 V, whereas a higher voltage is actually required in practical circumstances. The extra overpotentials mainly come from the devices and intrinsic activation barriers of electrodes.³ The electrode also involves slow reaction kinetics that limit the hydrogen production rate, such as reactants adsorption/desorption, electric contact, and gas-involving interface.³ Therefore the practical water electrolysis confronts both electrode thermodynamic and kinetic issues.

The above situation necessitates active electrocatalysts to simultaneously reduce the operation overpotentials and to facilitate the reaction speed. To date, the noble metals (platinum groups) and noble oxides (Ru or Ir oxides) are demonstrated as the most active HER and OER electrocatalysts, respectively.^{3,4} However, their scarcity and high cost are major obstacles in the large-scale water splitting. Therefore, tremendous efforts are focused on exploiting inexpensive alternatives such as transition metal-based and metal-free materials.

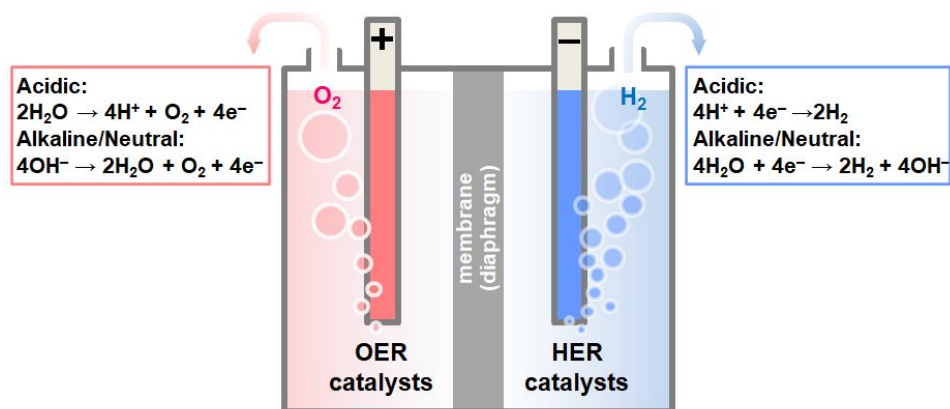


Figure 1. Scheme of conventional water electrolyzer with two half reactions under acidic and alkaline/neutral conditions.

In order to be economically attractive, it is preferred to conduct both half reactions of water splitting in the same electrolyte. If an electrocatalyst is active for both half HER and OER in the same electrolyte, it will further simplify the manufacture of a water splitting electrolyzer. Given the severe corrosion and/or poor activity of most 1st-row transition metal-based electrocatalysts for OER in strongly acidic electrolytes, there is a growing interest in developing so-called bifunctional electrocatalysts for overall water splitting at high pH. Herein, we summarize the recent advances of nonprecious electrocatalysts for overall water splitting with a particular emphasis on alkaline electrolytes. Several representative catalyst categories, including transition metal phosphides, chalcogenides, oxides, nitrides, carbides, borides, alloys, and even metal-free materials, are highlighted. Several designing strategies for improving activities are also discussed with the aim of providing guidance in designing new electrocatalysts. Finally, our perspective on the current challenges and future opportunities of water splitting driven by low-cost and competent electrocatalysts are included.

2. Representative nonprecious and bifunctional electrocatalysts

2.1 Transition metal phosphides

Benefiting from high conductivity, metallic character, and the electronegativity of P sites to trap protons,⁵ transition metal phosphides have recently emerged as promising nonprecious alternatives to noble metals and oxides based electrocatalysts for overall water splitting. To date, a large number of transition metal phosphides electrocatalysts have been developed by using the strategies of phosphorization, metal-doping and theoretical calculations. According to the number

of metal elements, the reported transition metal phosphides electrocatalysts can be generally grouped into three main categories: mono metal phosphides, binary metal phosphides, and ternary metal phosphides.

Mono metal phosphides such as Co-P, Ni-P, Fe-P, Mo-P, and Cu-P, have been widely used as efficient bifunctional electrocatalysts for overall water splitting due to the facile preparation method, earth-abundant material, and outstanding performance. Transition metal-based phosphides (TMPs) have long been utilized as hydroprocessing catalysts in chemical industry.⁶ A notable example is Ni₂P, which was first theoretically predicted and later experimentally proved to be capable of catalyzing HER.^{7,8} Subsequently, many TMPs including those based on Co, Fe and Cu, have been explored as promising HER electrocatalysts.^{9-12,13} For instance, Sun et al. investigated the electrodeposited Co-P films as the bifunctional electrocatalysts for both HER and OER under alkaline conditions.¹⁴ Using CoSO₄ and NaH₂PO₂ as the Co and P sources, respectively, amorphous Co-P films were prepared via potentiodynamic deposition method (Figure 2a). Linear sweep voltammetry (LSV) of Co-P exhibited the HER catalytic onset potential of -50 mV versus reversible hydrogen electrode (vs RHE) as shown in Figure 2b. Even though its onset potential was slightly more negative than that of Pt-C, the behaviors of Co-P surpassed Pt-C beyond -167 mV vs RHE (Figure 2b). Moreover, Co-P materials could also be directly applied for OER. As shown in Figure 2c, Co-P produced a current density of 10 mA cm⁻² at an overpotential of 345 mV and rivaled the performance of IrO₂ as measured under the same OER condition. Post electrocatalysis characterization revealed that the in situ formed cobalt oxides and (oxy)hydroxides were most likely the real OER active species on Co-P. When Co-P was utilized as electrocatalyst for both cathode and anode, it only required a voltage of 1.744 V to deliver 100 mA cm⁻² in a two-electrode configuration (Figure 2d). Recently, Hu et al. reported a Ni₂P-based Janus electrocatalyst for overall water splitting, which generated 10 mA cm⁻² at 1.63 V during serving as both cathode and anode catalysts under alkaline conditions.¹⁵

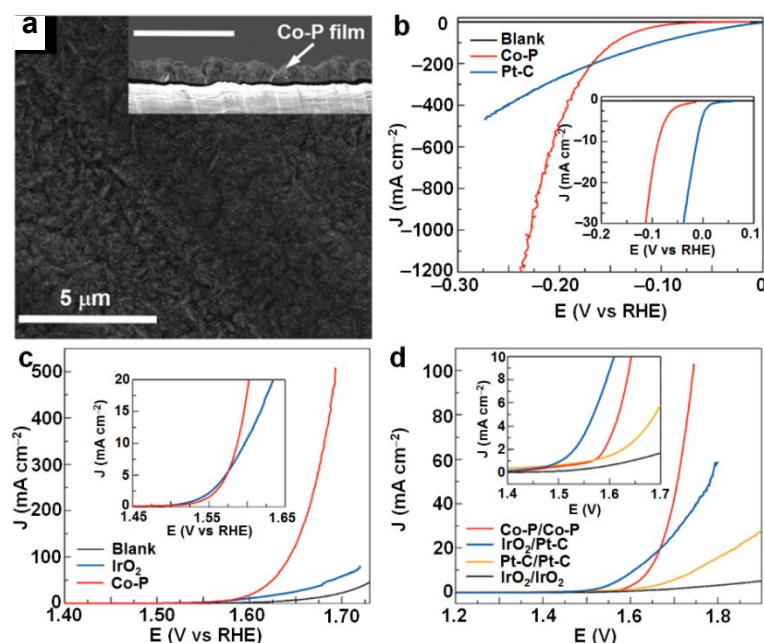


Figure 2 (a) SEM image of electrodeposited Co-P film (inset: cross section SEM image). LSV curves of Co-P, Pt-C and blank Cu foil for HER (b), OER (c), and overall water splitting (d) in 1.0 M KOH (insets: expanded LSV onset regions). Reproduced from ref. 14. Copyright 2015 John Wiley & Sons, Inc.

In order to enhance the intrinsic activity of mono metal phosphides materials, the extrinsic metal-doping methodology has been well developed for fabricating efficient binary metal phosphides and ternary metal phosphides water splitting electrocatalysts.¹⁶⁻²¹ For example, Du et al. introduced molybdenum into nickel phosphide nanosheets on carbon nanotubes ($\text{Ni}_1\text{Mo}_1\text{P NSs@MCNTs}$), as shown in Figure 3a).¹⁶ The reported binary metal phosphides exhibited excellent overall water splitting performance with a low cell voltage of 1.601 V to drive 10 mA cm^{-2} (Figure 3b). The abundant micropores and defects in the hierarchical structure of $\text{Ni}_1\text{Mo}_1\text{P NSs@MCNTs}$ were proposed to provide the active sites and facilitate mass/ion diffusion. A series of Co-doped nickel phosphides (NiCoP) bifunctional catalysts were reported by Qu, Ma, Chang and co-workers.²² As shown in Figure 4a, the NiCoP hybrids on reduced graphene oxide showed a catalytic current density of 10 mA cm^{-2} at 1.59 V for overall water splitting. Combining electrochemical measurements with density functional theory (DFT) calculations (Figure 4b), it revealed that Co-doping modulated the surface active sites, accelerated the charge transfer, and boosted their superior catalytic activity. Subsequently, Tang et al. developed a Ni-Co-Cu ternary metal phosphide heterostructure ($\text{NiCoP@Cu}_3\text{P}$) for water splitting. Due to the multiple synergistic effects of the ternary catalyst, it exhibited an enhanced catalytic performance for both HER and OER in alkaline solution.²³

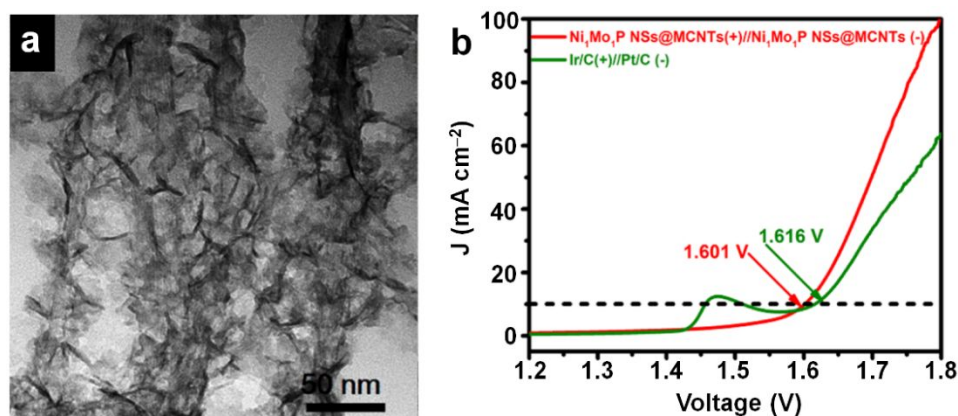


Figure 3 (a) TEM image of $\text{Ni}_1\text{Mo}_1\text{P NSs@MCNTs}$. (b) LSV curves of $\text{Ni}_1\text{Mo}_1\text{P NSs@MCNTs(+)//Ni}_1\text{Mo}_1\text{P NSs@MCNTs(-)}$ and Ir/C(+)//Pt/C(-) catalyst couples for overall water splitting. Electrolyte: 1.0 M KOH; scan rate: 5 mV s^{-1} . Reproduced from ref.16. Copyright 2018, American Chemical Society.

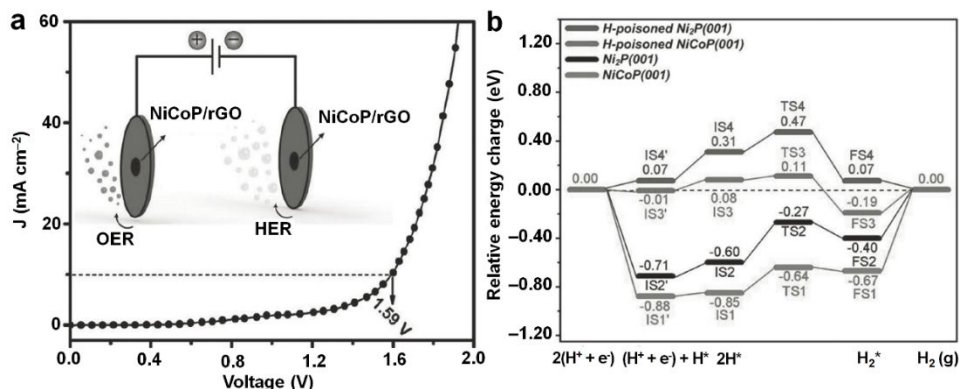


Figure 4 (a) LSV curve of NiCoP/rGO for overall water splitting in 1.0 M KOH at a scan rate of 5 mV s^{-1} . Inset shows the schematic overall water splitting in a two-electrode configuration. (b) Calculated energy profiles for HER on pristine and H-poisoned NiCoP (0001) and Ni₂P (001) facets. The relative energies are plotted with respect to the energy change in the reaction of $2(\text{H}^+ + \text{e}^-) \rightarrow \text{H}_2$. Reproduced from ref. 22. Copyright 2016 John Wiley & Sons, Inc.

2.2 Transition metal chalcogenides

Transition metal chalcogenides including sulfides and selenides, have attracted considerable attention for enhanced electrocatalytic HER and OER applications owing to their rich electrochemical properties.²⁴ By hybridizing with the nonprecious transition metals such as Ni, Co, Fe, and alloys,^{25–34} a variety of transition metal chalcogenides based electrocatalysts have been explored for overall water-splitting.

In 2015, Zou et al. synthesized Ni₃S₂ nanosheet arrays on nickel foam (NF) via direct hydrothermal sulfurization of NF using thiourea as a source of sulfur (denoted Ni₃S₂/NF).³⁵ The resultant Ni₃S₂/NF delivered a current density of 10 mA cm^{-2} at quite low overpotentials of 223 and 260 mV for HER (Figure 5a) and OER (Figure 5b), respectively. DFT computations revealed that the exposed high-index facets of Ni₃S₂ decreased the coordination number of Ni and S sites and lowered the free energy of intermediate H* adsorption (ΔG_{H^*}), which was beneficial to the overall HER performance (Figure 5c). Meanwhile, the energy barriers for critical OER steps were also decreased (Figure 5d). By electrochemical desulfurization of iron sulfide supported on iron foam, Zhang et al. reported FeS/IF electrocatalysts for high-performance alkaline overall water-splitting (Figure 6a).²⁸ The high catalytic activity of FeS/IF was attributed to the following advantages (Figure 6b): (i) the self-supported, hierarchical, and metallic scaffold (FeS/IF) rendered abundant active site on the catalyst surface and excellent conductivity; (ii) the superaerophobicity of Fe@FeO_xS_y promoted mass diffusion at the multi-phase interfaces; and (iii) the higher intrinsic activity of Fe@FeO_xS_y was the most important factor for HER and enhanced the overall water splitting performance.

In addition to the above examples, Sun et al. reported in situ growth of NiSe nanowires on NF (NiSe/NF) under hydrothermal condition. The as-prepared 3D NiSe/NF electrocatalysts exhibited high catalytic activity and durability for both OER and HER under alkaline condition. In a two electrode configuration, this bifunctional alkaline water electrolyzer enabled 10 mA cm^{-2} under a

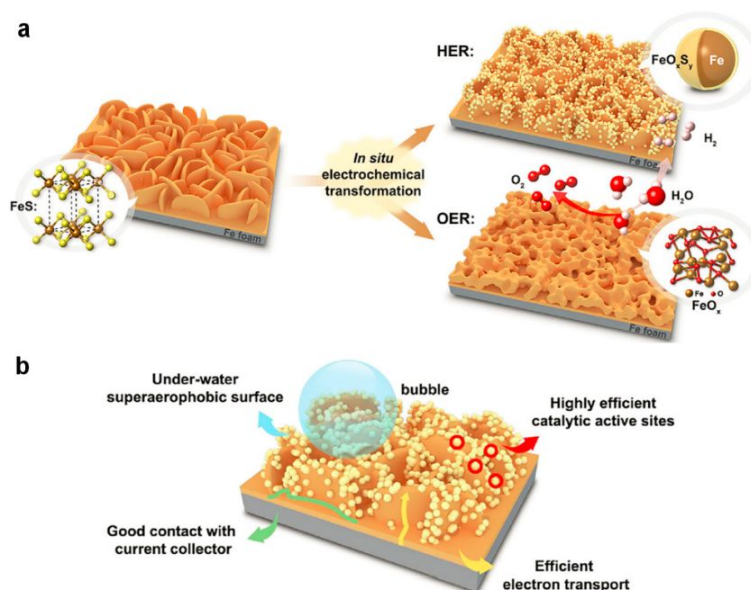


Figure 6 (a) Scheme of in situ transforming FeS/IF pre-catalyst into Fe-H₂cat for HER and Fe-O₂cat for OER. (b) Scheme of several key factors contributed to the highly active Fe-H₂cat. Reproduced from ref. 28 Copyright 2018 Elsevier.

2.3 Transition metal oxides

Because of their low cost, high intrinsic activity, and robust stability, transition metal-based oxides (TMOs) have provided a promising possibility in developing bifunctional catalysts with efficient electrocatalytic.^{37,38,39} For instance, Cui and co-workers reported an unconventional top-down electrochemical lithiation method to prepare ultra-small diameter transition metal oxide (iron, cobalt, nickel oxides and their mixed oxides) nanoparticles on carbon nanofibers (Figure 7a-e).⁴⁰ As shown in HRTEM images (Figure 7f-g), CoO-based TMO nanoparticles gradually changed from single crystalline nanoparticles (~20 nm) to interconnected crystalline fragments (2-5 nm). The grain boundaries of the interconnected TMO nanoparticles created additional active sites and also ensured strong interconnection, which maintained good contacts and increased the catalytic activity. In bifunctional water-splitting experiments, the NiFeO_x nanoparticles produced a current density of 10 mA cm⁻² at only 1.51 V, surpassing the IrO₂/Pt couple in 1.0 M KOH. It's worth noting that large number of electrochemical lithiation cycles may break off the particles and lead to negative effects on the catalytic performance of TMOs (Figure 7h).

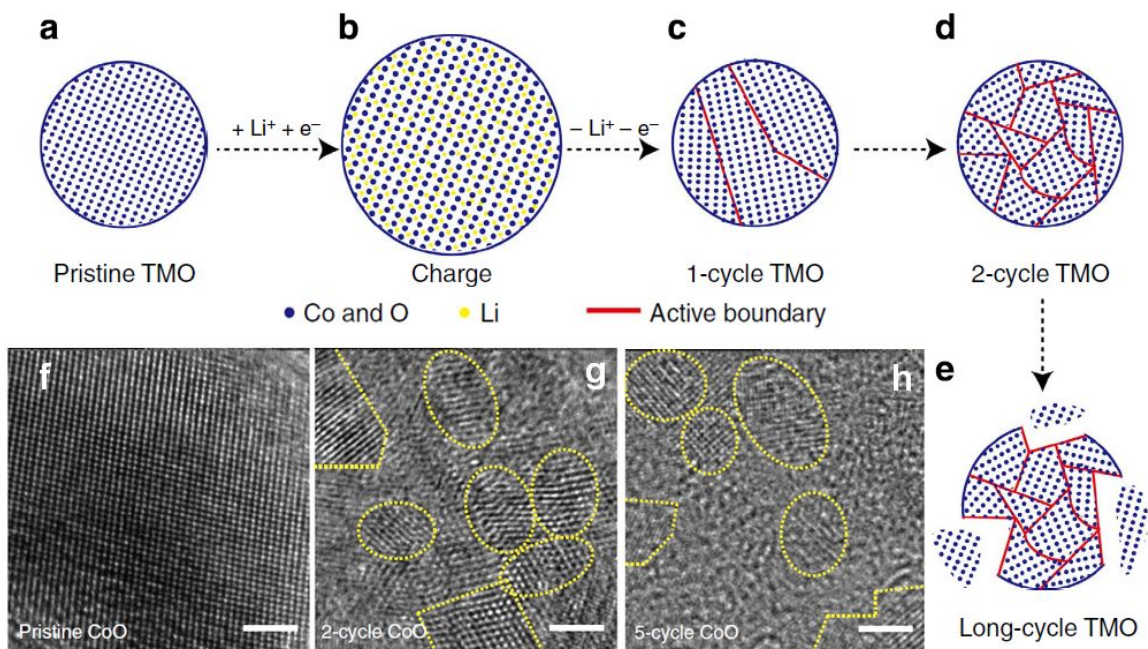


Figure 7 (a-e) Schematic of morphology evolution of TMO under galvanostatic cycles. The TMO particles gradually change from single crystalline to ultra-small interconnected crystalline nanoparticles. HRTEM images of (f) pristine, (g) 2-cycle, and (h) 5-cycle carbon nanofiber supported CoO (CoO/CNF). Scale bar: 2 nm. Reproduced from ref. 40. Copyright 2015 Nature Publishing Group.

The ABO_3 -type perovskite materials have emerged as a new category of efficient TMOs electrocatalysts for overall water splitting, due to their intriguing chemical, physical, and catalytic properties.^{41,42} In 2011, Shao-Horn et al. reported the $Ba_{0.5}Sr_{0.5}Co_{0.8}Fe_{0.2}O_{3-\delta}$ perovskites electrocatalysts exhibiting a higher OER activity than that of the state-of-the-art iridium oxide in alkaline media.⁴³ This work stimulated further efforts to optimize the electronic structures of perovskites for developing bifunctional water electrolysis materials.^{44-45,46} For instance, Ciucci and co-workers prepared a double perovskite oxide ($NdBaMn_2O_{5.5}$) with a better overall water splitting activity at large potentials (>1.75 V) and catalytic durability relative to those of $Pt/C-RuO_2$.⁴⁴ The outstanding catalytic performance was rationalized by the e_g orbit occupancy, optimized O p-band center location, and distorted structure.

Transition metal hydroxides/(oxy)hydroxides, as analogous to transition metal oxides, have also been demonstrated for efficient bifunctional overall water splitting,^{47,48} such as $Ni(OH)_2$,⁴⁹ $VOOH$,⁵⁰ $FeOOH$,⁵¹ and many bimetallic hydroxides.⁵²⁻⁵⁵ The metal original oxyhydroxides species or in situ formed metal oxyhydroxides from pristine catalysts were regarded as real active species for OER,⁵⁶ and they were also active for HER by facilitating water dissociation as rate-limiting step.⁵⁷ In 2018, Driess reported a nickel phosphate ($Ni_{11}(HPO_3)_8(OH)_6$) bifunctional electrocatalyst with remarkable activity and excellent stability both on nickel foam (NF) and on fluorine doped tin oxide in alkaline media (Figure 8a).⁵⁸ *In situ* and *ex situ* spectroscopic techniques were employed to characterize the formation of nickel oxyhydroxide active sites for

both OER and HER half-reaction (Figure 8b). As shown in Figure 8c, $\text{Ni}_{11}(\text{HPO}_3)_8(\text{OH})_6$ catalyst required a low overpotential of 121 mV to reach 10 mA cm^{-2} at the cathode, comparable to that of Pt catalyst. At the anode, it delivered 10 mA cm^{-2} at the overpotential of 232 mV and surpassed those of noble RuO_2 and IrO_2 catalysts (Figure 8d). During using as an overall water splitting bifunctional electrocatalyst, it showed a low cell voltage of 1.6 V at 10 mA cm^{-2} in alkaline media.

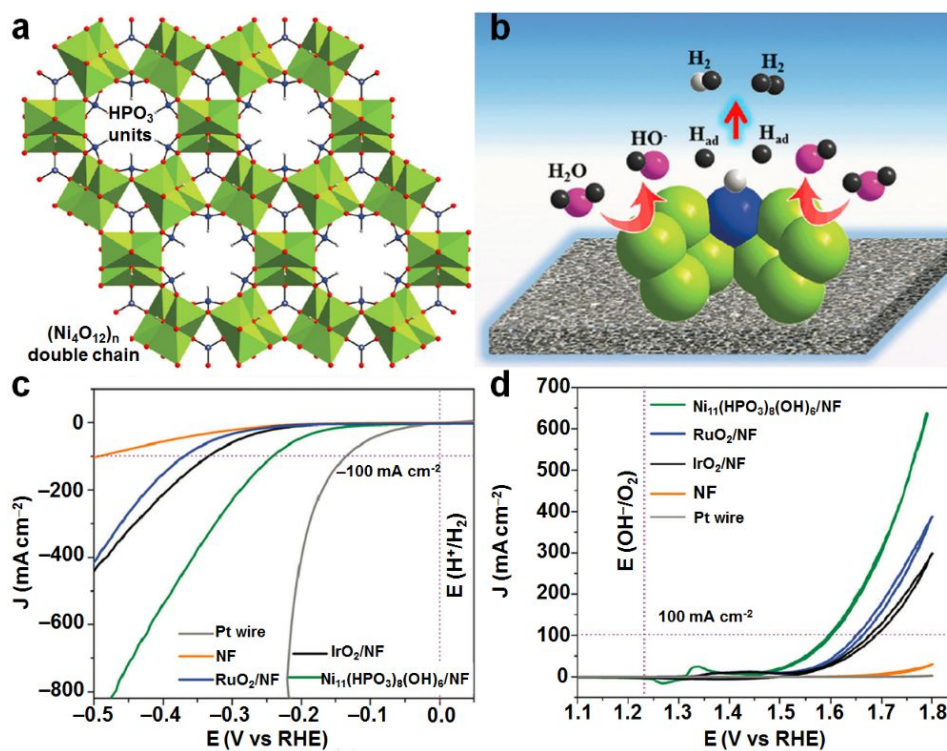


Figure 8 (a) Crystal structure of nickel phosphite (P: blue, O: red, H: grey). (b) Schematic illustration of HER on nickel phosphite (nickel octahedral: chartreuse, phosphite: blue, H: grey). Electrocatalytic performances of nickel phosphite supported on Ni foam (NF) compared with noble metal-based catalysts in 1.0 M KOH: (c) LSV curves for HER (scan rate: 5 mV s^{-1}) and (d) cyclic voltammogram plots for OER (scan rate: 1 mV s^{-1}). Reproduced from ref. 58. Copyright 2018 The Royal Society of Chemistry.

2.4 Transition metal nitrides

Transition metal-based nitrides (TMNs) are interstitial compounds where nitrogen atoms integrated into interstitial sites. The electronic redistributions of TMNs improve the conductivity, catalytic efficiency, and long-term stability.^{59,60} A number of TMNs have been prepared through nitridation method by tuning the structural and electronic environment around the metal centers,^{61,62} such as nickel nitride,^{63,64} Co-V nitride,⁶⁵ Ni-Mo nitride,^{66,67} Ti-N,⁶⁸ and Ni-Fe nitride.⁶⁹ In 2015, Shalom et al. reported a nickel nitride electrocatalyst for both HER and OER by growing nickel nitride (Ni_3N) on Ni-foam.⁶⁴ The increase of active Ni^{2+} species and *in situ* formation of Ni hydroxides led to its enhanced electrocatalytic activity for water splitting. By

encapsulating the Ni-Fe nitrides in reduced graphene oxide, Yao et al. developed a bimetallic Ni₃FeN/r-GO catalyst through a one-step nitridation process with alginate hydrogels (Figure 9a).⁷⁰ As-prepared Ni₃FeN/r-GO alkaline electrolyzer could generate 10 mA cm⁻² at 1.60 V with a long durability. Theoretical calculations revealed that the reduced ΔG_{H^*} on Ni₃FeN(111) and the redistributed charge at interfaces between Ni₃FeN and r-GO contributed to high HER activity (Figure 9b). The optimized binding energies on Ni₃FeN benefited to the enhanced OER activity (Figure 9c). Recently, a multi-step synthetic strategy was reported by Chou et al. for fabricating hierarchical Ni-Fe-Mo tri-metal nitrides through room-temperature Fe incorporation and NH₃ thermal treatment (Figure 9d).⁷¹ The prepared Ni-Fe-Mo catalysts drove 10 mA cm⁻² at 1.513 V in a two electrode cell, outperforming most of the reported bifunctional catalysts.

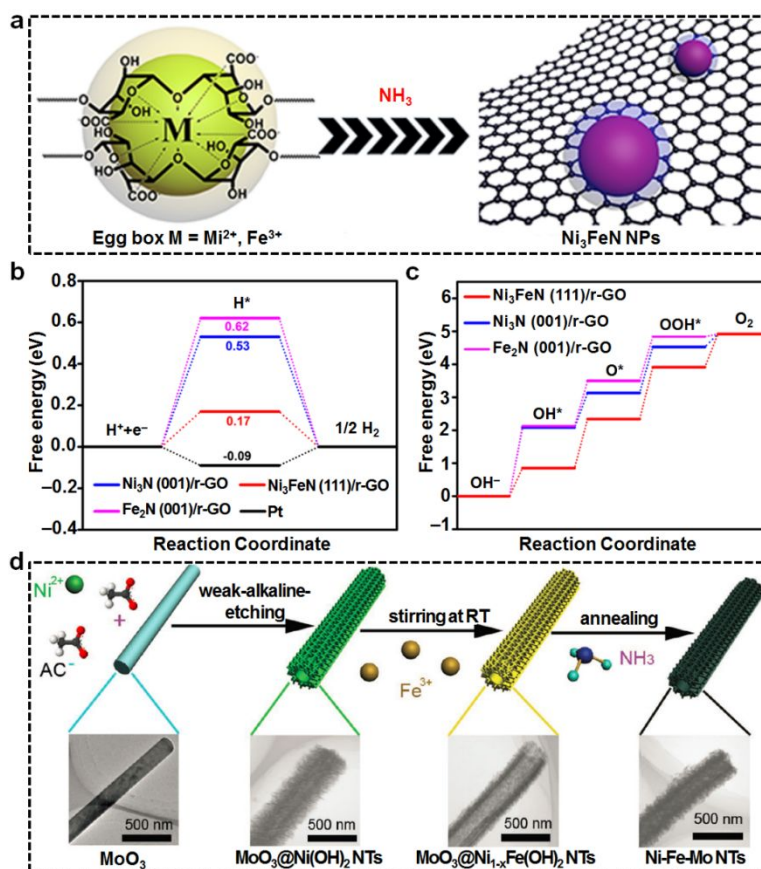


Figure 9 (a) Schematic synthesis of Ni₃FeN/r-GO derived from sodium alginate with r-GO hydrogels. Schematic free energy profiles for (b) OER and (c) HER. (d) Schematic synthesis of Ni-Fe-Mo nitride nanotubes. Figures 9a-9c Reproduced from ref. 70. Copyright 2018 American Chemical Society. Figure 9d Reproduced from ref. 71. Copyright 2018 John Wiley & Sons, Inc.

2.5 Transition metal carbides

Transition metal-based carbides (TMCs) display similar electronic and catalytic properties to Pt-group metals, which have been actively reported as promising electrocatalysts for HER and OER applications.⁷²⁻⁸¹ Generally, chemical/physical vapor deposition (CVD), electrochemical

deposition and pyrolysis of metal complexes are mainly three kinds of methods to prepare TMCs such as Mo, W, Fe, Ni carbides.⁸²⁻⁸⁶ Gao et al. synthesized a Mo₂C bifunctional electrocatalyst supported on carbon sheets (Mo₂C@CS) by a one-pot pyrolysis of glucose and ammonium molybdate (Figure 10).⁸⁷ Benefitting from the synergistic effects between Mo₂C and carbon sheets, the Mo₂C@CS catalyst exhibited superior activity for both HER and OER. In order to improve the relatively weak OER activities of metal carbides, the strategy of inducing other species such as Co⁸⁶ and NiFe alloys,⁸⁸ has been developed as an effective way to enhance the overall water splitting performance. For instance, Lin and co-workers prepared MoC₂-doped NiFe alloy nanoparticles via one-step calcination process.⁸⁸ The hybrid bifunctional electrocatalysts achieved overall water-splitting current density of 10 mA cm⁻² at a low potential of 1.53 V in alkaline media, surpassing the precious Pt/C//RuO₂ counterpart.

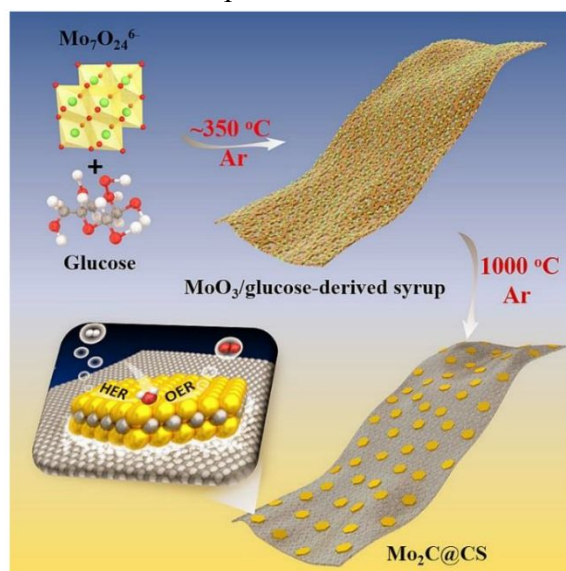


Figure 10 Schematic synthesis of Mo₂C@CS. Reproduced from ref. 87. Copyright 2017 John Wiley & Sons, Inc.

2.6 Transition metal borides

Transition metal borides are intermetallic compounds with electron-deficient boron element. The low electronegativity characteristic of boron allows transition metal borides present unusual structural and chemical properties.⁸⁹ The presence of boron is capable of reducing the hydroxylation reaction barrier, which stimulates the research efforts to explore the transition metal borides based electrocatalysts for overall water splitting.⁹⁰⁻⁹⁵ In particular, both amorphous and crystalline transition metal borides have been reported as efficient bifunctional catalysts for both the HER and OER. For instance, Schuhmann et al. reported amorphous cobalt boride (Co₂B) electrocatalyst using chemical reduction of CoCl₂ with NaBH₄.⁹⁰ In a two-electrode cell water electrolysis, the optimized Co₂B achieved a current density of 10 mA cm⁻² at 1.61 V on an inert support and at 1.59 V when impregnated with nitrogen-doped graphene. Geyer and co-workers prepared crystalline boride rich FeB₂ nanoparticles by chemical reduction of Fe²⁺ using LiBH₄ (Figure 11a).⁹¹ For OER, the formation of the FeOOH/FeB₂ heterojunction facilitated its catalytic

activity (Figure 11b, c). Theoretical calculations revealed that the boron-rich surface regulated the binding energy for chemisorption and desorption of hydrogen-containing intermediates, enhancing the HER performance (Figure 11d, e). In overall water splitting experiments, the FeB₂ electrolyzer delivered a current density of 10 mA cm⁻² at a low cell voltage of 1.57 V (Figure 11f).

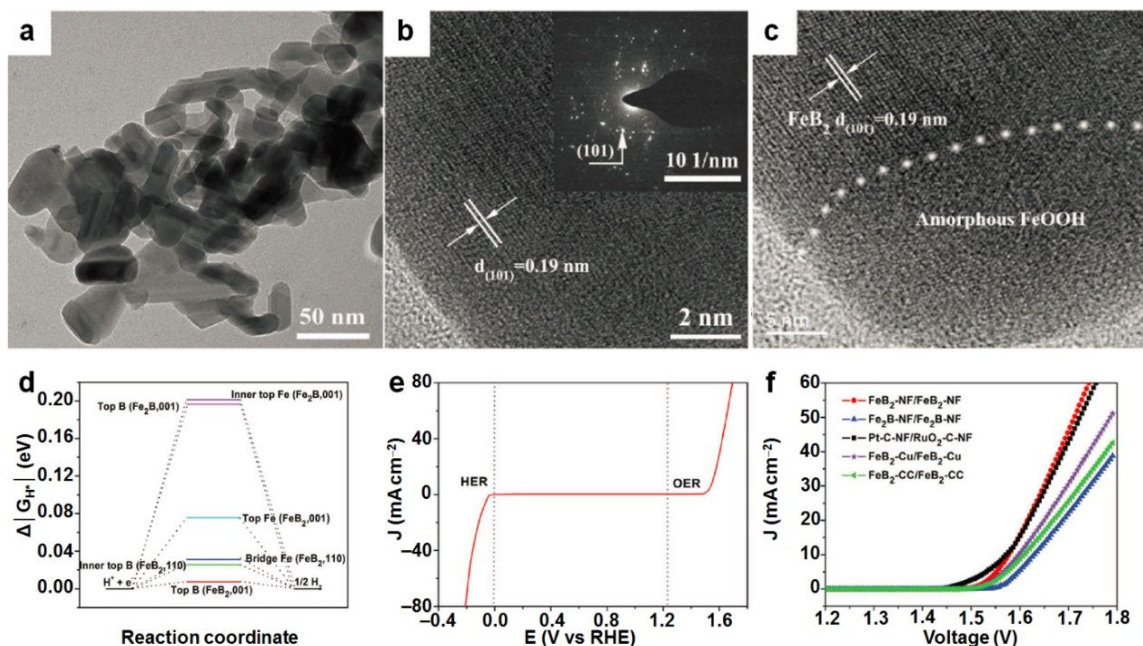


Figure 11 (a-b) TEM images of FeB₂. (c) HRTEM image of FeB₂ after OER for 12 h. (d) Calculated free energy diagram of HER on (001) and (110) facets of FeB₂ and Fe₂B at equilibrium potential. (e) LSV curves for HER and OER in a three-electrode configuration. (f) LSV curves of overall water splitting in a two-electrode configuration. Reproduced from ref. 91. Copyright 2017 John Wiley & Sons, Inc.

2.7 Transition metal alloys

Transition metal alloys comprising two or more metallic elements, possess many intriguing advantages of unusual and attractive crystallographic and electronic properties for heterogeneous water splitting catalysis.⁹⁶⁻⁹⁸ For instance, Li et al. prepared Fe-Co alloy films on carbon fiber papers via one-step electroreductive deposition (Figure 12a, b).⁹⁹ By tuning the ratio of precursor metals, the optimized Fe_{0.4}Co_{0.6} film exhibited excellent OER activity with a low overpotential of 283 mV at 10 mA cm⁻², which was better than precious IrO₂ catalyst (Figure 12c). Another Fe_{0.45}Co_{0.55} film displayed high HER activity showing an overpotential of 163 mV at 10 mA cm⁻² (Figure 12d). During using as bifunctional catalysts for overall water splitting, Fe_{0.45}Co_{0.55} composite films exhibited a low voltage of 1.68 V at 10 mA cm⁻² (Figure 12e). The *in situ* generated metallic hydroxides/oxides and the metals are beneficial for efficient OER and HER, respectively. Very recently, Driess and co-workers synthesized the atomically ordered intermetallic CoSn₂ nanocrystals using a solution chemistry method, which showed excellent catalytic activity and long-term stability for OER, HER, and overall water-splitting in alkaline media (Figure 13).¹⁰⁰ The post characterization of CoSn₂ revealed that the OER process in alkaline

media leached a large amount of Sn from the CoSn_2 crystal lattices and simultaneously oxidized Co to $\text{CoO}_x/\text{CoOOH}$ as active species. In contrast, during electrocatalytic HER, only a slight loss of Sn from the surface occurs, exposing the active Co^0 to protons. The co-existence of Co (as catalytically active center) and Sn (superior electrical conductor) in CoSn_2 nanocrystals led to highly efficient catalytic performance and long-term stability.

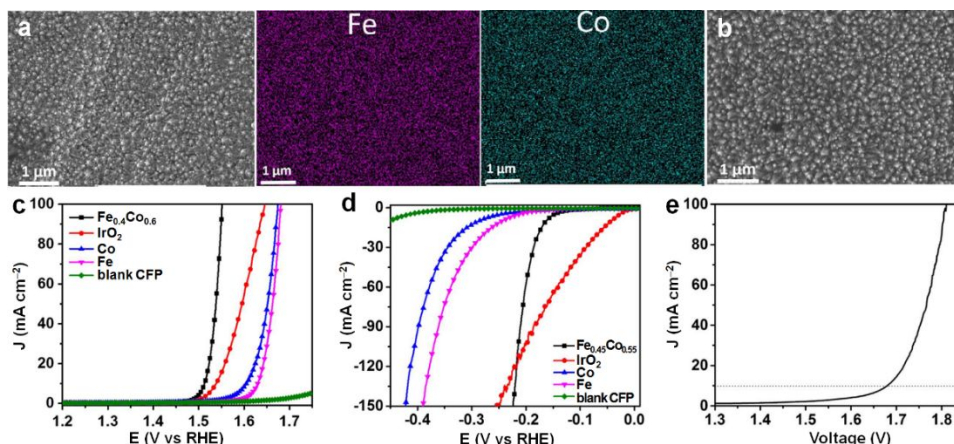


Figure 12 (a) SEM image with elemental mapping of $\text{Fe}_{0.4}\text{Co}_{0.6}$ composite films for OER. (b) SEM image of $\text{Fe}_{0.4}\text{Co}_{0.6}$ composite film for HER. LSV curves of OER (c), HER (d), and overall water splitting (e) in 1.0 M KOH. Scan rate: 1 mV s^{-1} . Reproduced from ref. 99. Copyright 2017 Elsevier.

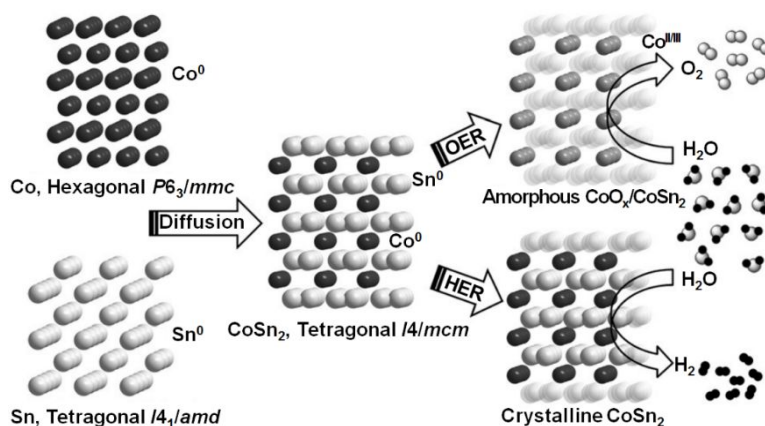


Figure 13 Unit cell structures of Co (black), Sn (light gray), and CoSn_2 (mixed black and light gray) and the structural modification of CoSn_2 during OER and HER in strongly alkaline media. Reproduced from ref. 100. Copyright 2018 John Wiley & Sons, Inc.

2.8 Carbon-based metal-free catalysts

Because of their low cost, mechanical/chemical stability, and structural flexibility, carbon-based metal-free materials have been developed as efficient electrocatalysts for overall water splitting.¹⁰¹⁻¹⁰³ To improve the catalytic activity, co-doping with other elements such as N, S, and P via bottom-up annealing or post treatments methods have been reported.^{104,105} For instance, Dai et al. prepared two-dimensional N, S co-doped graphitic sheets (SHG) with a unique hierarchical

structure (Figure 14a-b).¹⁰⁶ The two-electrode water splitting polarization of the SHG-based cell showed a potential of 1.70 V to deliver 10 mA cm⁻² at the initial stage, followed by a stable \approx 1.68 V for continuous operation (Figure 14c). After the long-term operation over 19 h, the catalytic behaviors of SHG-based cell outperformed the Pt/RuO₂ combination (Figure 14d). The outstanding catalytic performance of SHG was rationalized by its unique architecture with a large surface area, rich active sites, and good electron/electrolyte transport properties.

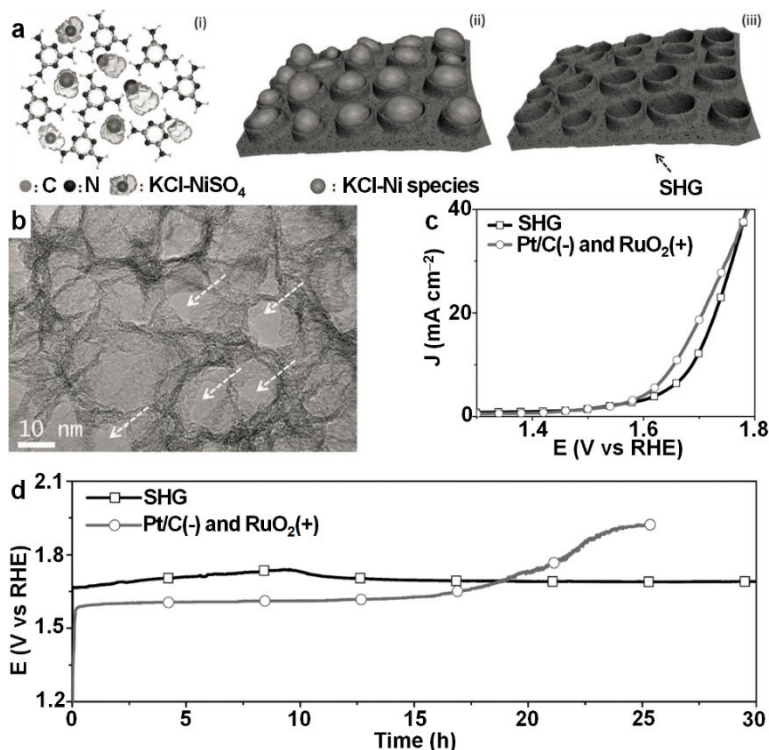


Figure 14 (a) Schematic synthesis for N, S co-doped graphitic sheets (SHG): (i) mixture of melamine, nickel sulfate, and KCl formed by ball milling; (ii) in situ growth of Ni-KCl@SHG; (iii) formation of SHG by etching the Ni@KCl and KCl seeds. (b) TEM image of SHG. (c) LSV curves of SHG and Pt/C-RuO₂ catalyst couples for overall water splitting in 1.0 M KOH at a scan rate of 10 mV s⁻¹. (d) Chronopotentiometry curves of overall water splitting electrolysis catalyzed by SHG and Pt/C-RuO₂ couples with a constant current density of 10 mA cm⁻² in 1.0 M KOH. Reproduced from ref. 106. Copyright 2017 John Wiley & Sons, Inc.

3. Designing strategies

Based on the above achievements for efficient bifunctional water splitting, a variety of designing strategies have been employed for improving the activity of electrocatalysts. Herein, we divide the reported designing strategies into the following categories, including: anion/cation regulation, carbon incorporation or encapsulation, the introducing of defects and vacancies, and interfacial engineering. In this section, we highlight the rational designing of these strategies with representing typical examples.

3.1 Anion/cation regulation

Anion/cation regulation has been considered as a promising strategy to modify electronic structure and catalytic activity of water splitting electrocatalysts by enhancing the free carrier density and increasing the active sites.¹⁰⁷⁻¹¹⁰ As shown in Figure 15a, Wu and co-workers synthesized a N-anion decorated Ni_3S_2 catalyst via a one-step calcination method for the bifunctional water splitting.¹⁴¹ A notably low cell voltage of 1.48 V was achieved to deliver 10 mA cm^{-2} in an overall water-splitting device by using N- Ni_3S_2 as electrocatalyst. N anions regulated the morphology and electronic structure of Ni_3S_2 and afforded the optimized Gibbs free-energy (ΔG_{H^*}) for HER (Figure 15b) and water adsorption energy ($\Delta G_{\text{H}_2\text{O}^*}$) for OER (Figure 15c).

In addition to anion modulation, metal cation doping has also been intensively investigated to explore high performance electrocatalysts.¹¹¹⁻¹¹³ For instance, the Mo dopants in CoP catalyst decreased ΔG_{H^*} for HER (Figure 15d),¹¹¹ and reduced the energy barrier in rate-limiting step for OER (Figure 15e). The Mo-doped CoP catalyst exhibited a low cell voltage of 1.56 V to generate 10 mA cm^{-2} for overall water splitting, outperforming than that of the Pt/C-Ir/C cell.

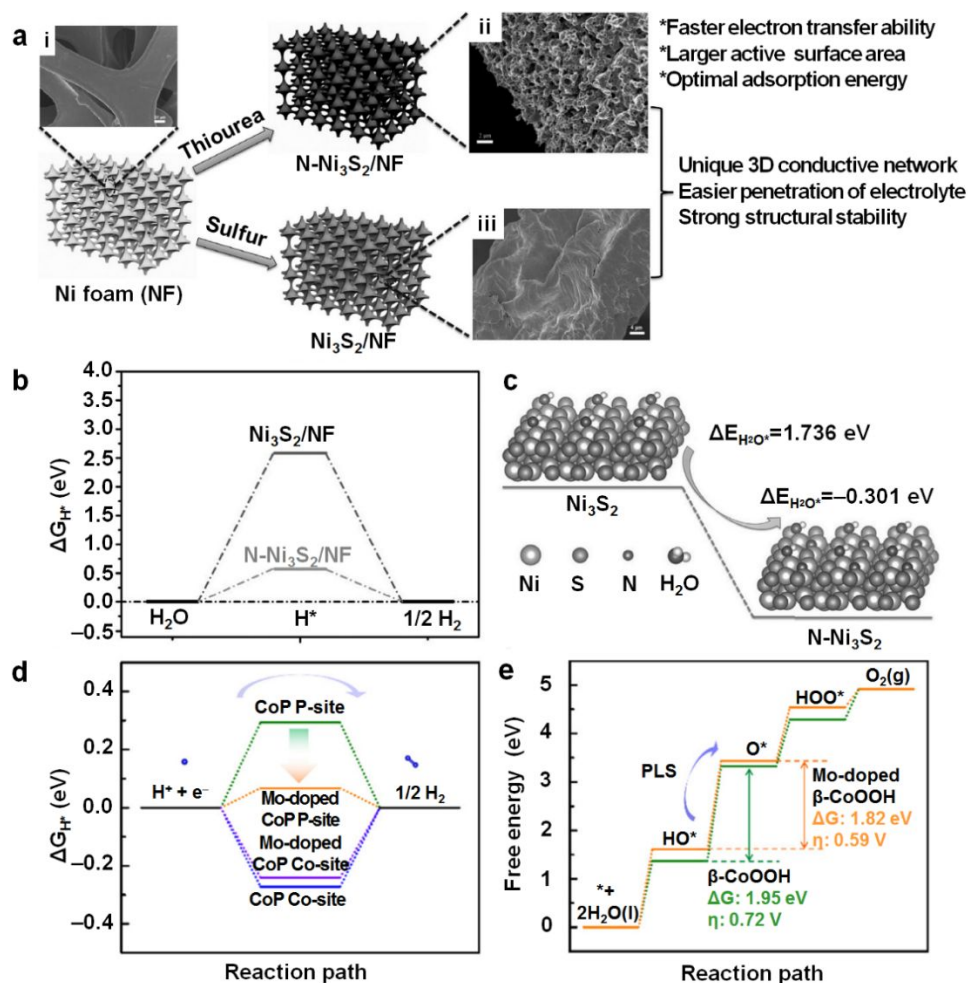


Figure 15 (a) Schematic synthesis of N-decorated Ni_3S_2 and pristine Ni_3S_2 grown on Ni foam substrate with the corresponding SEM images of NF (i), N- $\text{Ni}_3\text{S}_2/\text{NF}$ (ii), and $\text{Ni}_3\text{S}_2/\text{NF}$ (iii). (b-c) Calculated hydrogen (b) and water (c) adsorption energies on N- Ni_3S_2 and Ni_3S_2 . Calculated

hydrogen adsorption free energy on pristine and Mo-doped CoP. (e) Calculated OER steps on pristine and Mo-doped β -CoOOH. Figures 15a-15c Reproduced from ref. 141. Copyright 2017 John Wiley & Sons, Inc. Figures 15d-15e Reproduced from ref. 111. Copyright 2018 Elsevier.

3.2 Carbon incorporation or encapsulation

The unique structure and intrinsic properties of nanocarbon substrates such as high conductivity, high surface area, and high chemical stability, make them as attractive substrates for developing efficient electrocatalysts.^{114,115} In the past a few years, many kinds of electrocatalysts consisting of nanocarbon substrates such as graphene and carbon nanotube, have been reported for overall water splitting. In 2013, Loh et al. prepared a graphene oxide and copper-centered metal organic framework electrocatalyst, showing an enhanced electrocatalytic properties and stability for both HER and OER.¹¹⁶

Doping nanocarbons with other elements such as N, P, S, and B, could improve the synergistic effect between active sites and carbon substrates providing an effective way to explore high-performance electrocatalysts.¹¹⁷⁻¹²⁰ For instance, Wang and co-workers reported cobalt-cobalt oxide/N-doped carbon ($\text{CoO}_x\text{@CN}$) electrocatalysts through one-pot thermal treatment method (Figure 16a-b).¹²¹ Benefiting from the high conductivity of carbon and the synergistic effect of metallic cobalt/cobalt oxide, $\text{CoO}_x\text{@CN}$ hybrids exhibited remarkable overall water splitting performance with a cell voltage of 1.55 V at 20 mA cm^{-2} . As illustrated in Figure 17a-b, Zhang et al. fabricated N, B-codoped graphitic carbon decorated cobalt hybrid electrocatalysts (Co/NBC) via a simple solvothermal method.¹²² In an overall water splitting cell, the optimized Co/NBC-900 hybrid showed outstanding bifunctional electrocatalytic activity and long-term stability (Figure 17c, a cell voltage of 1.68 V to drive 10 mA cm^{-2}). DFT calculations revealed that the synergistic effects between cobalt-cobalt oxide and N, B-codoped carbon substrates optimized the adsorption/desorption energies of hydrogen and oxygen intermediates for HER and OER, respectively (Figure 17d).

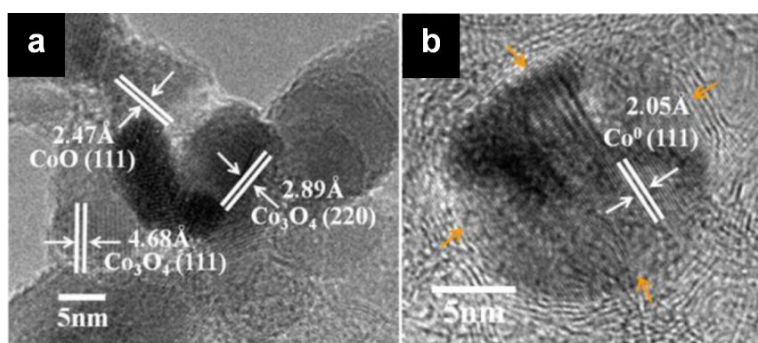


Figure 16 (a, b) HRTEM images of $\text{CoO}_x\text{@CN}$. The brown arrows in (b) point at the graphitic carbon layers. Reproduced from ref. 121. Copyright 2015 American Chemical Society.

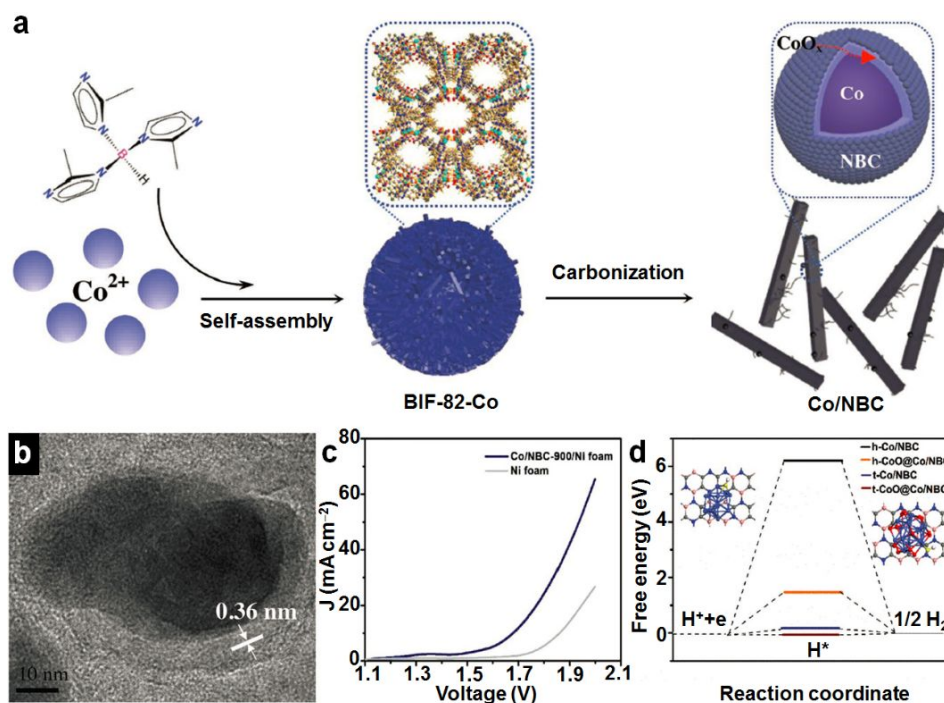


Figure 17 (a) Schematic synthesis of Co/NBC. (b) HRTEM image of Co/NBC-900. (c) LSV curves of overall water splitting in 1.0 M KOH with a scan rate of 5 mV s⁻¹. (d) Calculated hydrogen adsorption free energy on Co/NBC-900 and other control samples. Reproduced from ref. 122. Copyright 2018 John Wiley & Sons, Inc.

3.3 Introduction of defects and vacancies

Defect structures, such as lattice defects, interstitial atoms, and vacancies, widely exist in various nanomaterials.¹²³ Some defects are believed to modify the electronic structures and provide additional active sites for electrocatalysts. For example, lattice defects in two dimensional (2D) transition metal dichalcogenides expose abundant edge sites for electrocatalysis.^{124,125} Another case is that topological defects in nanocarbon is believed to be able to tailor catalytic performances.¹²³

Anion vacancies in transition metal compounds, such as oxygen¹²⁶ and sulfur vacancies,¹²⁷ are capable of modulating electronic configuration of catalysts and thus improving the catalytic performances. For instance, O vacancies (V_O) created by plasma in Co_3O_4 were found to be beneficial for its OER activity.¹²⁸ More interestingly, V_O could be filled again by P atoms via plasma treatment to enhance its HER activity as well. The filled P atoms significantly modulated the electronic structure of Co_3O_4 and altered binding energies of the reactant intermediates to improve its overall water splitting performance.

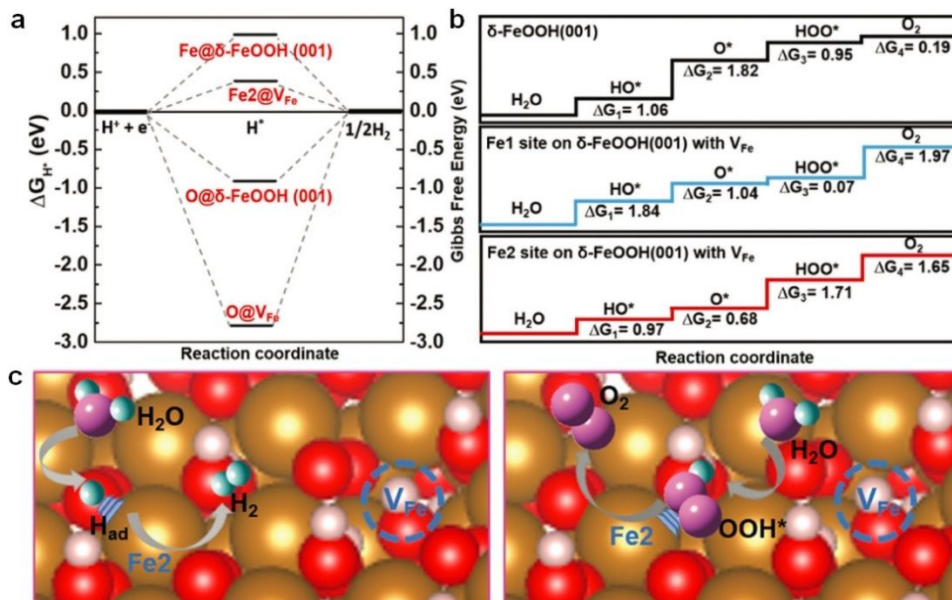


Figure 18 Calculated free energy diagrams of HER (a) and OER (b) on δ -FeOOH. (c) Schematic illustration of HER (left) and OER (right) on the Fe2 site of δ -FeOOH with an adjacent iron vacancy (brown: Fe; red: O). Reproduced from ref. 51. Copyright 2018 John Wiley & Sons, Inc.

Similarly, an alternative option of modifying electrocatalyst is to create metal vacancies, even though this option has been challenged by the high formation energies of most metal vacancies.¹²³ In order to tackle this issue, a facile wet-chemistry method was developed to prepare δ -FeOOH nanosheets with Fe vacancies (V_{Fe}).⁵¹ Theoretical calculations revealed that V_{Fe} strengthened the binding between H and O (Figure 18a, c), which adversely weakened the activity on neighboring Fe site (Fe1 site). In contrast, the second Fe atom (Fe2 site) was activated due to the optimized ΔG_{H^*} value. Analogous situation was found for the OER process, wherein it was Fe2, rather than the Fe1 site, that was triggered due to a moderate binding affinity towards the oxygen intermediates (Figure 18b). Additionally, the electronic conductivity of δ -FeOOH was also improved with the existence of V_{Fe} , which was beneficial to its electrocatalytic performance as well.

3.4 Interfacing engineering

Recent years have witnessed the increasing interest in nano interfaces among heterostructures and hybrid compounds because of the generated synergetic effects between different moieties to tailor the electronic structures of catalysts.¹²⁹ The modulated electronic structure in turn influences the overall performance in electrocatalysis.¹³⁰ For instance, the interfaces between MoS_2 and Ni_3S_2 facilitated the adsorption of both hydrogen and oxygen intermediates and consequently improved the HER and OER activities of MoS_2/Ni_3S_2 heterostructure.¹³¹ It can be rationally anticipated that increasing the number of nano interfaces would enhance the catalytic performances of electrocatalysts and thus such a strategy has been increasingly adopted. For example, N integration into $NiMoO_4$ precursor could increase the interfaces in the final product $NiMoO_4/NiS_2$ during the sulfurization process. The N dopants was found to promote Ni atoms to

diffuse outward and to form epitaxial NiS_2 (Figure 19a), resulting in a unique $\text{N-NiMoO}_4/\text{NiS}_2$ nanowire/nanosheet heterostructure (Figure 19b).¹³² Besides, N dopants also optimized the lattice matching between NiS_2 and N-NiMoO_4 by altering the crystal lattice fringes (Figure 19c) and creating O vacancies, which also increased the number of interfaces (Figure 19d). Consequently, electrons were transferred from N-NiMoO_4 to NiS_2 , optimizing the H adsorption on NiS_2 for higher HER activity. This was accompanied by the increased valance state of Ni in N-NiMoO_4 , resulting in higher OER activity. The N atom itself also optimized the chemical adsorption of both H^+ and OH^- intermediates on NiMoO_4 and the electronic conductivity of the electrocatalyst. As expected, the $\text{N-NiMoO}_4/\text{NiS}_2$ catalyst couple required a low cell voltage of only 1.60 V to reach a catalytic current density of 10 mA cm^{-2} for overall water splitting electrolysis.

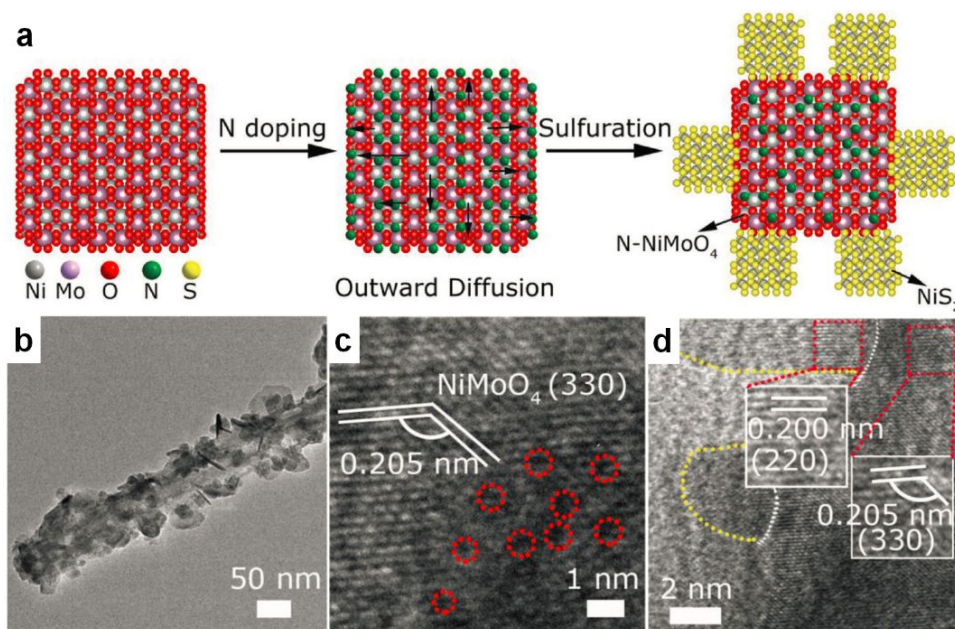


Figure 19 (a) Schematic growth of $\text{N-NiMoO}_4/\text{NiS}_2$. (b) TEM and (c, d) HRTEM image of $\text{N-NiMoO}_4/\text{NiS}_2$. Reproduced from ref.132. Copyright 2018 John Wiley & Sons, Inc.

4. Conclusions and outlook

Along with the continuous interest in exploring renewable and sustainable energy resources, developing bifunctional electrocatalysts for overall water splitting may bring an effective method in producing clean hydrogen for the future energy portfolio. This minireview showcases recent progress in developing nonprecious and bifunctional electrocatalysts for overall water splitting under alkaline conditions, including transition metal phosphides, chalcogenides, oxides, nitrides, carbides, borides, alloys, as well as metal-free catalysts. All the representative work discussed herein has been compiled in Table 1. Besides, some modification strategies in improving HER and OER performances are introduced and discussed, such as heteroatom modification, carbon incorporation, defect creation, and interfacing engineering.

Despite the above exciting achievements, there still exists a large space for further improvement as well as some unresolved issues. First, the mechanistic understanding of each step

in water splitting electrolysis necessitates in-depth characterization and investigation. In fact, structural changes and true active sites during HER and OER at high pH still remain ambiguous, as redox prefeatures are often observed. Therefore, in situ spectroscopic studies are highly recommended to provide direct evidence regarding the operating mechanisms of water splitting utilizing bifunctional electrocatalysts, which in turn is believed to guide the rational design of new electrocatalysts.¹³³ Second, the design strategy for competent bifunctional electrocatalysts requires further improvement. The nature of two distinctive active sites for the two half redox reactions (HER and OER) of water splitting renders it challenging to design a single electrocatalyst active for both reactions. Most of the prevalent modification strategies are limited to a narrow range of materials, whereas a universal strategy applicable for various compositions is highly preferred. Especially for practical applications at an industrial scale, well-controlled, low-cost and environmentally friendly synthesis is desirable. In addition to catalytic bifunctionality, the sufficient long-term stability of electrocatalysts operating at large current density (e.g., 1 A cm⁻²) is another critical factor for commercial electrolyzers, which has received much less attention till today. It requires not only high corrosion tolerance under extreme conditions but also robust adhesion to current collectors. At present, only self-supported catalysts have demonstrated the catalytic performance at large current density, such as Ni foam- or Fe foam-based transition metal catalysts.^{134,135} Third, the development of bifunctional electrocatalysts functioning in a wide pH range is still in the infancy stage. It is mainly restricted by the poor tolerance of most 1st-row transition metal-based OER electrocatalysts in low pH electrolytes. Even though neutral pH electrolytes bear the best environmental friendliness, most electrocatalysts exhibit mediocre efficiency for both HER and OER at pH 7, probably due to the low conductivity of neutral electrolytes. Although a few examples of low-cost electrocatalysts have been reported with performances superior to those of noble metal-based counterparts,^{136,137} most bifunctional electrocatalysts cannot compete the integrated noble metal-based electrocatalyst couples for overall water splitting. We hope this review will bring useful guidance and motivation to our peers in developing innovative and competent bifunctional electrocatalysts for hydrogen production from water splitting electrolysis.

Table 1 Comparison of representative bifunctional electrocatalysts for overall water splitting.

Catalyst	Electrolyte	η_{HER} at j (mV@mA cm ⁻²)	HER Tafel slope (mV dec ⁻¹)	η_{OER} at j (mV@mA cm ⁻²)	OER Tafel slope (mV dec ⁻¹)	Overall voltage at j (V@mA cm ⁻²)
Phosphides						
Ni ₂ P ¹⁵	1.0 M KOH	220@10	–	290@10	47	1.63@10
Co-P film ¹⁴	1.0 M KOH	94@10	42	345@10	47	1.744@100
Ni-P film ¹³⁸	1.0 M KOH	93@10	43	344@10	49	1.67@10
Cu ₃ P ¹²	0.1 M KOH	222@10	148	412@50	63	–
MoP/NF ¹³⁹	1.0 M KOH	114@10	54.6	265@10	56.6	1.62@10
Ni ₁ Mo ₁ P NSs@MCNTs ¹⁶	1.0 M KOH	135@10	137.5	255@10	45.1	1.601@10
NiCoP/rGO ²²	1.0 M KOH	209@10	124.1	270@10	65.7	1.59@10
Mo-CoP ¹¹¹	1.0 M KOH	13@10	65	305@10	56	1.56@10
Co-P/NC ¹⁴⁰	1.0 M KOH	154@10	51	319@10	52	2.0@165
Chalcogenides						
h-NiS _x ²⁵	1.0 M KOH	60@10	99	180@10	96	1.47@10
FeS/IF ²⁸	1.0 M KOH	300@100	77	238@10	82.7	1.65@10
Ni _x Co _{3-x} S ₄ /Ni ₃ S ₂ /NF ³⁰	1.0 M KOH	500@719	107	160@10	95	1.58@10
Ni ₃ S ₂ /NF ³⁵	1.0 M KOH	223@10	–	260@10	–	–
N-Ni ₃ S ₂ /NF ¹⁴¹	1.0 M KOH	110@10	–	350@170	70	1.48@10
MoS ₂ /Ni ₃ S ₂ ¹³¹	1.0 M KOH	110@10	83	218@10	88	1.56@10
Co ₃ Se ₄ ³¹	1.0 M KOH	–	–	397@320	44	1.59@10
NiSe/NF ³²	1.0 M KOH	96@10	120	270@20	64	1.63@10
NiSe-NiO _x ¹⁴²	1.0 M KOH	160@10	–	243@10	128	1.68@10
Oxides						
NiFeO _x /CFP ⁴⁰	1.0 M KOH	88@10	–	250@10	31.5	1.51@10
VOOH ⁵⁰	1.0 M KOH	164@10	104	270@10	68	1.62@10
δ-FeOOH NSs/NF ⁵¹	1.0 M KOH	108@10	68	265@10	36	1.62@10
NiFe LDH/Ni foam ⁵²	1.0 M NaOH	210@10	–	240@10	–	1.7@10

FePO ₄ /NF ⁵³	1.0 M KOH	123@10	104.5	218@10	42.7	1.54@10
Co-Mn carbonate hydroxide ⁵⁴	1.0 M KOH	180@10	–	294@30	–	1.68@10
Ni ₁₁ (HPO ₃) ₈ (OH) ₆ ⁵⁸	1.0 M KOH	42@10	102	232@10	91	1.6@10
SrCo _{0.85} Fe _{0.1} P _{0.05} O _{3-δ} ⁴⁵	1.0 M KOH	110@10	94	310@10	55	1.52@10
Nitrides						
Co ₄ N-VN _{1-x} O _x /CC ⁶⁵	1.0 M KOH	118@10	73.6	263@10	64.1	1.64@10
TiN@Ni ₃ N ⁶⁸	1.0 M KOH	21@10	42.1	350@10	93.7	1.64@10
Ni ₃ FeN/r-GO-20 ⁷⁰	1.0 M KOH	213@10	90	270@10	54	1.60@10
Ni-Fe-MoN NTs ⁷¹	1.0 M KOH	55@10	109	228@10	41	1.513@10
Carbides						
Mo ₂ C@CS ⁸⁷	1.0 M KOH	178@10	82	320@10	98	1.73@10
Co ₄ Mo ₂ @NC/Ti ¹⁴³	1.0 M KOH	218@10	73.5	330@10	48.7	1.74@10
Borides						
FeB ₂ ⁹¹	1.0 M KOH	61@10	87.5	296@10	52.4	1.57@10
Alloys						
Fe-Co composite films ⁹⁹	1.0 M KOH	163@10	51	283@10	34	1.68@10
CoSn ₂ ¹⁰⁰	1.0 M KOH	103@10	78	230@10	89	1.55@10
Non-metal catalysts						
N,S-doped graphitic sheets ¹⁰⁶	0.1 M KOH	310@10	112	330@10	71	1.68@10
N/P/F tri-doped graphene ¹⁴⁴	0.1 M KOH	520@10	–	390@10	136	–
Other catalysts						
CoO _x @CN ¹²¹	1.0 M KOH	232@10	115	260@10	–	1.55@10
NiFe-MOF ¹⁴⁵	0.1 M KOH	134@10	–	240@10	34	1.55@10
Co/NBC-900 ¹²²	1.0 M KOH	117@10	146	302@10	70	1.68@10
P-Co ₃ O ₄ ¹²⁸	1.0 M KOH	120@10	52	280@10	51.6	1.76@50
N-NiMoO ₄ /NiS ₂ ¹³²	1.0 M KOH	99@10	74.2	283@10	44.3	1.60@10

Acknowledgement

Y.S. acknowledges the financial support of the Herman Frasch Foundation (820-HF17), National Science Foundation (CHE-1914546), and the University of Cincinnati.

References

- 1 J. M. Bockris and E. C. Potter, *J. Electrochem. Soc.*, 1952, **99**, 169-186.
- 2 L. Zhang, J. Xiao, H. Wang and M. Shao, *ACS Catal.*, 2017, **7**, 7855-7865.
- 3 T. Bak, J. Nowotny, M. Rekas and C. Sorrell, *Int. J. Hydrogen Energy*, 2002, **27**, 991-1022.
- 4 C. Tang, H.-F. Wang and Q. Zhang, *Acc. Chem. Res.*, 2018, **51**, 881-889.
- 5 Y. Shi and B. Zhang, *Chem. Soc. Rev.*, 2016, **45**, 1529-1541.
- 6 S. Carenco, D. Portehault, C. Boissiere, N. Mezailles and C. Sanchez, *Chem. Rev.*, 2013, **113**, 7981-8065.
- 7 P. Liu and J. A. Rodriguez, *J. Am. Chem. Soc.*, 2005, **127**, 14871-14878.
- 8 E. J. Popczun, J. R. McKone, C. G. Read, A. J. Biacchi, A. M. Wiltrout, N. S. Lewis and R. E. Schaak, *J. Am. Chem. Soc.*, 2013, **135**, 9267-9270.
- 9 E. J. Popczun, C. G. Read, C. W. Roske, N. S. Lewis and R. E. Schaak, *Angew. Chem. Int. Ed.*, 2014, **53**, 5427-5430.
- 10 P. Jiang, Q. Liu, Y. Liang, J. Tian, A. M. Asiri and X. Sun, *Angew. Chem. Int. Ed.*, 2014, **53**, 12855-12859.
- 11 J. F. Callejas, J. M. McEnaney, C. G. Read, J. C. Crompton, A. J. Biacchi, E. J. Popczun, T. R. Gordon, N. S. Lewis and R. E. Schaak, *ACS Nano*, 2014, **8**, 11101-11107.
- 12 J. Tian, Q. Liu, N. Cheng, A. M. Asiri and X. Sun, *Angew. Chem. Int. Ed.*, 2014, **53**, 9577-9581.
- 13 Z. Y. Zhang, S. S. Liu, J. Xiao and S. Wang, *J. Mater. Chem. A*, 2016, **4**, 9691-9699.
- 14 N. Jiang, B. You, M. Sheng and Y. Sun, *Angew. Chem. Int. Ed.*, 2015, **54**, 6251-6254.
- 15 L.-A. Stern, L. Feng, F. Song and X. Hu, *Energy Environ. Sci.*, 2015, **8**, 2347-2351.
- 16 H. Xu, J. Wei, K. Zhang, Y. Shiraishi and Y. Du, *ACS Appl. Mater. Interfaces*, 2018, **10**, 29647-29655.
- 17 Z. Zhao, D. E. Schipper, A. P. Leitner, H. Thirumalai, J.-H. Chen, L. Xie, F. Qin, M. K. Alam, L. C. Grabow and S. Chen, *Nano Energy*, 2017, **39**, 444-453.
- 18 H. Liang, A. N. Gandi, D. H. Anjum, X. Wang, U. Schwingenschlögl and H. N. Alshareef, *Nano Lett.*, 2016, **16**, 7718-7725.
- 19 J. Gao, L. Yang, D. Wang and D. P. Cao, *Chem. Eur. J.*, DOI: 10.1002/chem.201904337.
- 20 Y. T. Yan, J. H. Lin, J. Cao, S. Guo, X. H. Zheng, J. C. Feng and J. L. Qi, *J. Mater. Chem. A*, 2019, **7**, 24486-24492.
- 21 M. Q. Yao, H. H. Hu, B. L. Sun, N. Wang, W. C. Hu and S. Komarneni, *Small*, 2019, **15**, 1905201.
- 22 J. Li, M. Yan, X. Zhou, Z. Q. Huang, Z. Xia, C. R. Chang, Y. Ma and Y. Qu, *Adv. Funct. Mater.*, 2016, **26**, 6785-6796.
- 23 X. Ma, Y. Chang, Z. Zhang and J. Tang, *J. Mater. Chem. A*, 2018, **6**, 2100-2106.

- 24 J. D. Benck, T. R. Hellstern, J. Kibsgaard, P. Chakthranont and T. F. Jaramillo, *ACS Catal.*, 2014, **4**, 3957-3971.
- 25 B. You and Y. Sun, *Adv. Energy Mater.*, 2016, **6**, 1502333.
- 26 J. Dong, F.-Q. Zhang, Y. Yang, Y.-B. Zhang, H. He, X. Huang, X. Fan and X.-M. Zhang, *Appl. Catal. B*, 2018, **243**, 693-702.
- 27 J. Wang, H.-x. Zhong, Z.-l. Wang, F.-l. Meng and X.-b. Zhang, *ACS Nano*, 2016, **10**, 2342.
- 28 X. Zou, Y. Wu, Y. Liu, D. Liu, W. Li, L. Gu, H. Liu, P. Wang, L. Sun and Y. Zhang, *Chem*, 2018, **4**, 1139-1152.
- 29 J. Yu, G. Cheng and W. Luo, *J. Mater. Chem. A*, 2017, **5**, 15838-15844.
- 30 Y. Wu, Y. Liu, G.-D. Li, X. Zou, X. Lian, D. Wang, L. Sun, T. Asefa and X. Zou, *Nano Energy*, 2017, **35**, 161-170.
- 31 W. Li, X. Gao, D. Xiong, F. Wei, W. G. Song, J. Xu and L. Liu, *Adv. Energy Mater.*, 2017, **7**, 1602579.
- 32 C. Tang, N. Cheng, Z. Pu, W. Xing and X. Sun, *Angew. Chem. Int. Ed.*, 2015, **54**, 9351-9355.
- 33 R. Xu, R. Wu, Y. Shi, J. Zhang and B. Zhang, *Nano Energy*, 2016, **24**, 103-110.
- 34 C. Panda, P. W. Menezes, C. Walter, S. Yao, M. E. Miehllich, V. Gutkin, K. Meyer and M. Driess, *Angew. Chem. Int. Ed.*, 2017, **56**, 10506-10510.
- 35 L.-L. Feng, G. Yu, Y. Wu, G.-D. Li, H. Li, Y. Sun, T. Asefa, W. Chen and X. Zou, *J. Am. Chem. Soc.*, 2015, **137**, 14023-14026.
- 36 C. Panda, P. W. Menezes, C. Walter, S. Yao, M. E. Miehllich, V. Gutkin, K. Meyer and M. Driess, *Angew. Chem. Int. Ed.*, 2017, **56**, 10506-10510.
- 37 H. Jin, C. Guo, X. Liu, J. Liu, A. Vasileff, Y. Jiao, Y. Zheng and S.-Z. Qiao, *Chem. Rev.* 2018, **118**, 6337-6408.
- 38 M. W. Kanan, Y. Surendranath and D. G. Nocera, *Chem. Soc. Rev.*, 2009, **38**, 109-114.
- 39 Z. Y. Zhang, S. S. Liu, F. Xiao and S. Wang, *ACS Sustainable Chem. Eng.*, 2017, **5**, 529-536.
- 40 H. Wang, H. W. Lee, Y. Deng, Z. Lu, P. C. Hsu, Y. Liu, D. Lin and Y. Cui, *Nat. Commun.*, 2015, **6**, 7261.
- 41 A. Kojima, K. Teshima, Y. Shirai and T. Miyasaka, *J. Am. Chem. Soc.*, 2009, **131**, 6050-6051.
- 42 D. Chen, C. Chen, Z. M. Baiyee, Z. Shao and F. Ciucci, *Chem. Rev.*, 2015, **115**, 9869-9921.
- 43 J. Suntivich, K. J. May, H. A. Gasteiger, J. B. Goodenough and Y. Shao-Horn, *Science*, 2011, **334**, 1383-1385.
- 44 J. Wang, Y. Gao, D. Chen, J. Liu, Z. Zhang, Z. Shao and F. Ciucci, *ACS Catal.*, 2017, **8**, 364-371.
- 45 G. Chen, Z. Hu, Y. Zhu, B. Gu, Y. Zhong, H. J. Lin, C. T. Chen, W. Zhou and Z. Shao, *Adv. Mater.*, 2018, **30**, 1804333.
- 46 Y. Zhu, W. Zhou, Y. Zhong, Y. Bu, X. Chen, Q. Zhong, M. Liu and Z. Shao, *Adv. Energy Mater.*, 2017, **7**, 1602122.

- 47 H. Yin and Z. Tang, *Chem. Soc. Rev.*, 2016, **45**, 4873-4891.
- 48 H. Jin, C. Guo, X. Liu, J. Liu, A. Vasileff, Y. Jiao, Y. Zheng and S.-Z. Qiao, *Chem. Rev.* 2018, **118**, 6337-6408.
- 49 Z. Xing, L. Gan, J. Wang and X. Yang, *J. Mater. Chem. A*, 2017, **5**, 7744-7748.
- 50 H. Shi, H. Liang, F. Ming and Z. Wang, *Angew. Chem. Int. Ed.*, 2017, **56**, 573-577.
- 51 B. Liu, Y. Wang, H. Q. Peng, R. Yang, Z. Jiang, X. Zhou, C. S. Lee, H. Zhao and W. Zhang, *Adv. Mater.*, 2018, **30**, 1803144.
- 52 J. Luo, J.-H. Im, M. T. Mayer, M. Schreier, M. K. Nazeeruddin, N.-G. Park, S. D. Tilley, H. J. Fan and M. Grätzel, *Science*, 2014, **345**, 1593-1596.
- 53 L. Yang, Z. Guo, J. Huang, Y. Xi, R. Gao, G. Su, W. Wang, L. Cao and B. Dong, *Adv. Mater.*, 2017, **29**, 1704574.
- 54 T. Tang, W.-J. Jiang, S. Niu, N. Liu, H. Luo, Y.-Y. Chen, S.-F. Jin, F. Gao, L.-J. Wan and J.-S. Hu, *J. Am. Chem. Soc.*, 2017, **139**, 8320-8328.
- 55 L. Hui, Y. Xue, D. Jia, H. Yu, C. Zhang and Y. Li, *Adv. Energy Mater.*, 2018, **8**, 1800175.
- 56 S. Jin, 2017, *ACS Energy Lett.*, 2017, **2**, 1937-1938.
- 57 R. Subbaraman, D. Tripkovic, D. Strmcnik, K.-C. Chang, M. Uchimura, A. P. Paulikas, V. Stamenkovic and N. M. Markovic, *Science*, 2011, **334**, 1256-1260.
- 58 P. W. Menezes, C. Panda, S. Loos, F. Bunschei-Brunns, C. Walter, M. Schwarze, X. Deng, H. Dau and M. Driess, *Energy Environ. Sci.*, 2018, **11**, 1287-1298.
- 59 N. Han, P. Liu, J. Jiang, L. Ai, Z. Shao and S. Liu, *J. Mater. Chem. A*, 2018, **6**, 19912-19933.
- 60 S. Dong, X. Chen, X. Zhang and G. Cui, *Coordin. Chem. Rev.*, 2013, **257**, 1946-1956.
- 61 J. Xiong, W. Cai, W. Shi, X. Zhang, J. Li, Z. Yang, L. Feng and H. Cheng, *J. Mater. Chem. A*, 2017, **5**, 24193-24198.
- 62 J. Song, G. Li, F. Xiong and X. Gao, *J. Mater. Chem.*, 2012, **22**, 20580-20585.
- 63 Z.-Y. Wu, W.-B. Ji, B.-C. Hu, H.-W. Liang, X.-X. Xu, Z.-L. Yu, B.-Y. Li and S.-H. Yu, *Nano Energy*, 2018, **51**, 286-293.
- 64 M. Shalom, D. Ressnig, X. Yang, G. Clavel, T. P. Fellingner and M. Antonietti, *J. Mater. Chem. A*, 2015, **3**, 8171-8177.
- 65 S. Dutta, A. Indra, Y. Feng, H. Han and T. Song, *Appl. Catal. B*, 2019, **241**, 521-527.
- 66 F.-C. Shen, S.-N. Sun, Z.-F. Xin, S.-L. Li, L.-Z. Dong, Q. Huang, Y.-R. Wang, J. Liu and Y.-Q. Lan, *Appl. Catal. B*, 2019, **243**, 470-480.
- 67 A. Wu, Y. Xie, H. Ma, C. Tian, Y. Gu, H. Yan, X. Zhang, G. Yang and H. Fu, *Nano Energy*, 2018, **44**, 353-363.
- 68 Q. Zhang, Y. Wang, Y. Wang, A. M. Al-Enizi, A. A. Elzatahry and G. Zheng, *J. Mater. Chem. A*, 2016, **4**, 5713-5718.
- 69 B. Zhang, C. Xiao, S. Xie, J. Liang, X. Chen and Y. Tang, *Chem. Mater.*, 2016, **28**, 6934-6941.
- 70 Y. Gu, S. Chen, J. Ren, Y. A. Jia, C. Chen, S. Komarneni, D. Yang and X. Yao, *ACS Nano*, 2018, **12**, 245-253.
- 71 C. Zhu, Z. Yin, W. Lai, Y. Sun, L. Liu, X. Zhang, Y. Chen and S. L. Chou, *Adv. Energy*

- Mater.*, 2018, 1802327.
- 72 C. Wan, Y. N. Regmi and B. M. Leonard, *Angew. Chem. Int. Ed.*, 2014, **53**, 6407-6410.
- 73 J. Zhu, K. Sakaushi, G. Clavel, M. Shalom, M. Antonietti and T.-P. Fellingner, *J. Am. Chem. Soc.*, 2015, **137**, 5480-5485.
- 74 W.-F. Chen, C.-H. Wang, K. Sasaki, N. Marinkovic, W. Xu, J. Muckerman, Y. Zhu and R. Adzic, *Energy Environ. Sci.*, 2013, **6**, 943-951.
- 75 Y. Liu, G. Yu, G. D. Li, Y. Sun, T. Asefa, W. Chen and X. Zou, *Angew. Chem. Int. Ed.*, 2015, **54**, 10752-10757.
- 76 Y. N. Regmi, G. R. Waetzig, K. D. Duffee, S. M. Schmuecker, J. M. Thode and B. M. Leonard, *J. Mater. Chem. A*, 2015, **3**, 10085-10091.
- 77 Y. Zhao, K. Kamiya, K. Hashimoto and S. Nakanishi, *Angew. Chem. Int. Ed.*, 2013, **52**, 13638-13641.
- 78 D. V. Esposito, S. T. Hunt, Y. C. Kimmel and J. G. Chen, *J. Am. Chem. Soc.*, 2012, **134**, 3025-3033.
- 79 L. Ma, S. Sui and Y. Zhai, *J. Power Sources*, 2008, **177**, 470-477.
- 80 F. Kong, X. Fan, A. Kong, Z. Zhou, X. Zhang and Y. Shan, *Adv. Funct. Mater.*, 2018, 1803973.
- 81 H. Yang, S. Luo, X. Li, S. Li, J. Jin and J. Ma, *J. Mater. Chem. A*, 2016, **4**, 18499-18508.
- 82 Z. Kou, L. Zhang, Y. Ma, X. Liu, W. Zang, J. Zhang, S. Huang, Y. Du, A. K. Cheetham and J. Wang, *Appl. Catal. B*, 2019, **243**, 678-685.
- 83 B. Maribo-Mogensen, G. M. Kontogeorgis and K. Thomsen, *J. Phys. Chem. B*, 2013, **117**, 3389-3397.
- 84 C. A. Wolden, A. Pickerell, T. Gawai, S. Parks, J. Hensley and J. D. Way, *ACS Appl. Mater. Interfaces*, 2011, **3**, 517-521.
- 85 S. Chouzier, T. Czeri, M. Roy-Auberger, C. Pichon, C. Geantet, M. Vrinat and P. Afanasiev, *J. Solid State Chem.*, 2011, **184**, 2668-2677.
- 86 H.-M. Wang, X.-H. Wang, M.-H. Zhang, X.-Y. Du, W. Li and K.-Y. Tao, *Chem. Mater.*, 2007, **19**, 1801-1807.
- 87 H. Wang, Y. Cao, C. Sun, G. Zou, J. Huang, X. Kuai, J. Zhao and L. Gao, *ChemSusChem*, 2017, **10**, 3540-3546.
- 88 Q. Hu, X. Liu, B. Zhu, L. Fan, X. Chai, Q. Zhang, J. Liu, C. He and Z. Lin, *Nano Energy*, 2018, **50**, 212-219.
- 89 H. Chen and X. X. Zou, *Inorg. Chem. Front.*, 2020, DOI: 10.1039/D0QI00146E.
- 90 J. Masa, P. Weide, D. Peeters, I. Sinev, W. Xia, Z. Sun, C. Somsen, M. Muhler and W. Schuhmann, *Adv. Energy Mater.*, 2016, **6**, 1502313.
- 91 H. Li, P. Wen, Q. Li, C. Dun, J. Xing, C. Lu, S. Adhikari, L. Jiang, D. L. Carrol and S. M. Geyer, *Adv. Energy Mater.*, 2017, **7**, 1700513.
- 92 H. Vrubel and X. Hu, *Angew. Chem. Int. Ed.*, 2012, **51**, 12703-12706.
- 93 J. M. V. Nsanzimana, V. Reddu, Y. Peng, Z. Huang, C. Wang and X. Wang, *Chem. Eur. J.*, 2018, **24**, 18502-18511.
- 94 Y. Chen, G. Yu, W. Chen, Y. Liu, G.-D. Li, P. Zhu, Q. Tao, Q. Li, J. Liu and X. Shen, *J.*

- Am. Chem. Soc.*, 2017, **139**, 12370-12373.
- 95 T. Osaka, H. Ishibashi, T. Endo and T. Yoshida, *Electrochimica Acta.*, 1981, **26**, 339-343.
- 96 R. Cava, H. Takagi, H. Zandbergen, J. Krajewski, W. Peck Jr, T. Siegrist, B. Batlogg, R. Van Dover, R. Felder and K. Mizuhashi, *Nature*, 1994, **367**, 252-253.
- 97 M. Armbrüster, R. Schlögl and Y. Grin, *Sci. Technol. Adv. Mater.*, 2014, **15**, 034803.
- 98 X. Wang, X. Liu, C.-J. Tong, X. Yuan, W. Dong, T. Lin, L.-M. Liu and F. Huang, *J. Mater. Chem. A*, 2016, **4**, 7762-7771.
- 99 W. Liu, K. Du, L. Liu, J. Zhang, Z. Zhu, Y. Shao and M. Li, *Nano Energy*, 2017, **38**, 576-584.
- 100 P. W. Menezes, C. Panda, S. Garai, C. Walter, A. Guillet and M. Driess, *Angew. Chem. Int. Ed.*, 2018, **57**, 15237-15242.
- 101 D. S. Su, S. Perathoner and G. Centi, *Chem. Rev.*, 2013, **113**, 5782-5816.
- 102 B. Xiong, L. Chen and J. Shi, *ACS Catal.*, 2018, **8**, 3688-3707.
- 103 L. Zhang, J. Xiao, H. Wang and M. Shao, *ACS Catal.*, 2017, **7**, 7855-7865.
- 104 J. Zhang, L. Qu, G. Shi, J. Liu, J. Chen and L. Dai, *Angew. Chem. Int. Ed.*, 2016, **55**, 2230-2234.
- 105 Z. Y. Zhang, Z. R. Y, J. Wang, X. Tian, P. Xu, G. Q. Shi and S. Wang, *J. Mater. Chem. A*, 2017, **5**, 17064-17072.
- 106 C. Hu and L. Dai, *Adv. Mater.*, 2017, **29**, 1604942.
- 107 M. S. Faber, M. A. Lukowski, Q. Ding, N. S. Kaiser and S. Jin, *J. Phys. Chem. C*, 2014, **118**, 21347-21356.
- 108 D. Kong, J. J. Cha, H. Wang, H. R. Lee and Y. Cui, *Energy Environ. Sci.*, 2013, **6**, 3553-3558.
- 109 Q. Liu, J. Tian, W. Cui, P. Jiang, N. Cheng, A. M. Asiri and X. Sun, *Angew. Chem. Int. Ed.*, 2014, **53**, 6710-6714.
- 110 T. Liu, X. Ma, D. Liu, S. Hao, G. Du, Y. Ma, A. M. Asiri, X. Sun and L. Chen, *ACS Catal.*, 2016, **7**, 98-102.
- 111 C. Guan, W. Xiao, H. Wu, X. Liu, W. Zang, H. Zhang, J. Ding, Y. P. Feng, S. J. Pennycook and J. Wang, *Nano Energy.*, 2018, **48**, 73-80.
- 112 C. Tang, R. Zhang, W. Lu, L. He, X. Jiang, A. M. Asiri and X. Sun, *Adv. Mater.*, 2017, **29**, 1602441.
- 113 T. Liu, D. Liu, F. Qu, D. Wang, L. Zhang, R. Ge, S. Hao, Y. Ma, G. Du and A. M. Asiri, *Adv. Energy Mater.*, 2017, **7**, 1700020.
- 114 Y. P. Zhu, C. Guo, Y. Zheng and S.-Z. Qiao, *Acc. Chem. Res.*, 2017, **50**, 915-923.
- 115 Y. Yu, Y. Shi and B. Zhang, *Acc. Chem. Res.*, 2018, **51**, 1711-1721.
- 116 M. Jahan, Z. Liu and K. P. Loh, *Adv. Funct. Mater.*, 2013, **23**, 5363-5372.
- 117 J. Deng, P. Ren, D. Deng and X. Bao, *Angew. Chem. Int. Ed.*, 2015, **54**, 2100-2104.
- 118 M. Tavakkoli, T. Kallio, O. Reynaud, A. G. Nasibulin, C. Johans, J. Sainio, H. Jiang, E. I. Kauppinen and K. Laasonen, *Angew. Chem. Int. Ed.*, 2015, **54**, 4535-4538.
- 119 S. Wang, J. Wang, M. Zhu, X. Bao, B. Xiao, D. Su, H. Li and Y. Wang, *J. Am. Chem. Soc.*, 2015, **137**, 15753-15759.

- 120 Y. P. Zhu, C. Guo, Y. Zheng and S.-Z. Qiao, *Acc. Chem. Res.*, 2017, **50**, 915-923.
- 121 H. Jin, J. Wang, D. Su, Z. Wei, Z. Pang and Y. Wang, *J. Am. Chem. Soc.*, 2015, **137**, 2688-2694.
- 122 M. R. Liu, Q. L. Hong, Q. H. Li, Y. Du, H. X. Zhang, S. Chen, T. Zhou and J. Zhang, *Adv. Funct. Mater.*, 2018, 1801136.
- 123 D. Yan, Y. Li, J. Huo, R. Chen, L. Dai and S. Wang, *Adv. Mater.*, 2017, **29**, 1606459.
- 124 J. Xie, H. Zhang, S. Li, R. Wang, X. Sun, M. Zhou, J. Zhou, X. W. Lou and Y. Xie, *Adv. Mater.*, 2013, **25**, 5807-5813.
- 125 H. Wang, X. B. Li, L. Gao, H. L. Wu, J. Yang, L. Cai, T. B. Ma, C. H. Tung, L. Z. Wu and G. Yu, *Angew. Chem. Int. Ed.*, 2018, **57**, 192-197.
- 126 L. Zhuang, L. Ge, Y. Yang, M. Li, Y. Jia, X. Yao and Z. Zhu, *Adv. Mater.*, 2017, **29**, 1606793.
- 127 H. Li, C. Tsai, A. L. Koh, L. Cai, A. W. Contryman, A. H. Fragapane, J. Zhao, H. S. Han, H. C. Manoharan and F. Abild-Pedersen, *Nat. Mater.*, 2016, **15**, 48.
- 128 Z. Xiao, Y. Wang, Y.-C. Huang, Z. Wei, C.-L. Dong, J. Ma, S. Shen, Y. Li and S. Wang, *Energy Environ. Sci.*, 2017, **10**, 2563-2569.
- 129 Y. Wang, B. Kong, D. Zhao, H. Wang and C. Selomulya, *Nano Today*, 2017, **15**, 26-55.
- 130 S. Bai, C. Wang, M. Deng, M. Gong, Y. Bai, J. Jiang and Y. Xiong, *Angew. Chem. Int. Ed.*, 2014, **53**, 12120-12124.
- 131 J. Zhang, T. Wang, D. Pohl, B. Rellinghaus, R. Dong, S. Liu, X. Zhuang and X. Feng, *Angew. Chem. Int. Ed.*, 2016, **55**, 6702-6707.
- 132 L. An, J. Feng, Y. Zhang, R. Wang, H. Liu, G. C. Wang, F. Cheng and P. Xi, *Adv. Funct. Mater.*, 2018, 1805298.
- 133 Y. Jiao, Y. Zheng, M. Jaroniec and S. Z. Qiao, *Chem. Soc. Rev.*, 2015, **44**, 2060-2086.
- 134 Y. Liu, X. Liang, L. Gu, Y. Zhang, G. D. Li, X. X. Zou and J. S. Chen, *Nat. Commun.*, 2018, **9**, 2609.
- 135 J. Q. Zhang, X. Shang, H. Ren, J. Q. Chi, H. Fu, B. Dong, C. G. Liu and Y. M. Chai, *Adv. Mater.*, 2019, **31**, 1905107.
- 136 B. You, X. Liu, G. Hu, S. Gul, J. Yano, D.-e. Jiang and Y. Sun, *J. Am. Chem. Soc.*, 2017, **139**, 12283-12290.
- 137 F. Song, W. Li, J. Yang, G. Han, P. Liao and Y. Sun, *Nat. Commun.*, 2018, **9**, 4531.
- 138 N. Jiang, B. You, M. Sheng and Y. Sun, *ChemCatChem*, 2016, **8**, 106-112.
- 139 Y. Jiang, Y. Lu, J. Lin, X. Wang and Z. Shen, *Small Methods*, 2018, **2**, 1700369.
- 140 B. You, N. Jiang, M. Sheng, S. Gul, J. Yano and Y. Sun, *Chem. Mater.*, 2015, **27**, 7636-7642.
- 141 P. Chen, T. Zhou, M. Zhang, Y. Tong, C. Zhong, N. Zhang, L. Zhang, C. Wu and Y. Xie, *Adv. Mater.*, 2017, **29**, 1701584.
- 142 R. Gao, G.-D. Li, J. Hu, Y. Wu, X. Lian, D. Wang and X. Zou, *Catal. Sci. Technol.*, 2016, **6**, 8268-8275.
- 143 J. Jiang, Q. Liu, C. Zeng and L. Ai, *J. Mater. Chem. A*, 2017, **5**, 16929-16935.
- 144 J. Zhang and L. Dai, *Angew. Chem. Int. Ed.*, 2016, **55**, 13296-13300.

145 J. Duan, S. Chen and C. Zhao, *Nat. Commun.*, 2017, **8**, 15341.